


Cite this: *RSC Pharm.*, 2024, **1**, 1042

# Optimized albendazole-loaded nanostructured lipid carrier gel: a redefined approach for localized skin cancer treatment†

Chinmayee Khot,<sup>‡a</sup> Kaustubh Kolekar,<sup>‡a</sup> Swati Dabhole,<sup>a,b</sup> Akshay Mohite,<sup>a</sup>  
Sameer Nadaf,<sup>c</sup> Popat S. Kumbhar<sup>\*a</sup> and John Disouza <sup>\*a,d</sup>

The chief purpose of the current study is to fabricate nanostructured lipid carrier (NLC)-based gel for localized delivery of repurposed albendazole (ABZ) against skin cancer to reduce systemic and other organ-related side effects and enhance patient compliance. ABZ NLCs were constructed by the melt-emulsification ultrasonication method and optimized using Box-Behnken Design (BBD). The ABZ NLCs were analyzed for mean particle size, % entrapment efficiency (%EE), and zeta potential. Furthermore, an NLC-based gel was developed using optimized ABZ NLCs and the Carbopol-934 gelling agent and characterized for physical properties, viscosity, texture, *ex vivo* skin permeation, *in vitro* cytotoxicity, stability, etc. The optimized ABZ NLCs displayed a %EE of  $89.85 \pm 5.6\%$  and a particle size of  $176.5 \pm 7.3$  nm. The pH of the ABZ NLC-based gel developed using 1.0% w/v of Carbopol-934 was between 5.1 and 6.0. The viscosity of the optimized ABZ NLC-based gel was  $6.64 \pm 0.67$  Pa s. Besides, the NLC-based gel exhibited better and controlled ABZ release at pH 5.5 and 6.8 than the conventional ABZ gel. The *ex vivo* permeation of ABZ from NLCs and the NLC-based gel was 5.1 and 4.5-fold higher, respectively, than from the conventional gel. Notably, the *in vitro* cytotoxicity against B16F10 cells of ABZ NLCs was 1.7-fold and 2.2-fold higher than those of pure ABZ and the ABZ NLC-based gel. A negligible cytotoxicity of the developed formulations was seen in normal HaCaT cells (human epidermal cells), signifying the compatibility of these formulations with healthy cells. Moreover, the ABZ-incorporated NLCs and NLC gel remained stable for twelve weeks at  $4 \pm 2$  °C. Thus, the given research concludes that the NLC-loaded gel could be a harmless, efficient, and novel choice to treat skin cancer using repurposed ABZ.

Received 12th July 2024,  
Accepted 17th October 2024

DOI: 10.1039/d4pm00207e

rsc.li/RSCPharma

## Introduction

Cancer is a leading cause of death worldwide.<sup>1,2</sup> Skin cancer stands as one of the prevalent types of cancer, ranking 20th in terms of occurrence.<sup>3,4</sup> In the United States, around 100 000 new skin cancer cases are reported each year, leading to over 6850 deaths. Skin cancer primarily consists of melanomas, which originate from melanocytes and are highly lethal, and

non-melanoma skin cancers (NMSCs), including basal cell carcinoma (BCC) and squamous cell carcinoma (SCC), which are more common but less aggressive.<sup>5–9</sup>

Various strategies are utilized to treat skin cancers, including chemotherapy, immunotherapy, surgical interventions, and radiotherapy. Chemotherapy is commonly used for advanced skin cancers and may also serve as an adjuvant therapy alongside surgery. However, the effectiveness of many chemotherapeutic agents is limited due to their non-specific targeting of tumor cells, the development of multidrug resistance (MDR), recurrence of disease, severe side effects, and high treatment costs.<sup>10</sup> These disadvantages of chemotherapy necessitate the discovery of new drugs. The discovery of new drugs using a conventional (*de novo*) approach is a stringent, costly, and lengthy process accompanied by a poor success rate.<sup>11</sup>

Drug repurposing is observed to be a potential avenue for overcoming the hurdles in the path of the *de novo* drug discovery process. Numerous drugs from diverse pharmacological classes including antihelmintics have been reported to show anti-skin cancer activity.<sup>4,12</sup> Albendazole (ABZ) is a wide-

<sup>a</sup>Department of Pharmaceutics, Tatyasaheb Kore College of Pharmacy, Warananagar, Tal: Panhala, Dist: Kolhapur, Maharashtra, 416113, India.

E-mail: jidisouza@tkcpwarana.ac.in, pskumbhar@tkcpwarana.ac.in;  
Fax: +02328223501; Tel: +02328 223526

<sup>b</sup>Department of Pharmaceutics, Genesis Institute of Pharmacy, Sonyachi Shirol, Radhanagari, Maharashtra, 416212, India

<sup>c</sup>Bharati Vidyapeeth College of Pharmacy, Palus, Maharashtra 416310, India

<sup>d</sup>SYBES's Bombay Institute of Pharmacy and Research, Dombivli (East), Maharashtra, 421204, India

†Electronic supplementary information (ESI) available. See DOI: <https://doi.org/10.1039/d4pm00207e>

‡These authors contributed equally to this work.

ranging benzimidazole structured antihelmintic medication. It is usually used to cure a variety of parasitic worm infections in humans as well as in animals.<sup>13–15</sup> However, ABZ faces several oral solid route formulation related challenges, due to low aqueous solubility and  $pK_a$  that leads to a decrease in the dissolution rate, GI absorption, and bioavailability of ABZ. Moreover, systemic and other organ-related toxicities are other key hurdles in its delivery.<sup>16</sup> The lipophilic character of ABZ is responsible for achieving its passive permeation through the skin, making it an ideal candidate for topical utilization which can also eliminate the aforesaid drawbacks. Nevertheless, topical drug delivery through the skin is restricted by various skin barriers.<sup>17</sup> Therefore, there is a dire need to deliver it using a suitable nanoparticulate platform.

At present, a variety of nanocarriers (NCs) encompassing lipid-based NCs such as ethosomes, solid lipid nanoparticles, liposomes, niosomes, transferosomes, nanostructured lipid carriers (NLCs), *etc.* have been investigated for the adequate transportation of various anticancer therapeutic agents.<sup>18</sup> These systems aim to enhance drug solubility, improve bioavailability, and facilitate targeted delivery to tumor sites. However, several limitations persist in these approaches. For instance, conventional liposomes may suffer from rapid clearance from circulation, leading to reduced efficacy, while nanoparticles can face challenges related to scalability and stability. Additionally, micelles often require specific surfactants, which may not be suitable for all therapeutic agents. In contrast, our approach utilizes NLCs for skin cancer treatment, effectively addressing these limitations. NLCs enhance cargo loading, improve permeability, and allow for controlled cargo release. They exhibit greater kinetic stability and robust structure, mimicking the lipid matrix of the *stratum corneum*, which overcomes challenges associated with dermal delivery.<sup>19–21</sup> This topical delivery method circumvents pre-systemic metabolism and degradation of therapeutic agents in the gastrointestinal tract, resulting in greater accumulation of the drug at the tumor site. Furthermore, NLCs improve therapeutic effectiveness, safety, and patient adherence.<sup>22</sup> By enhancing drug delivery and mitigating the drawbacks of existing systems, our innovative formulation offers a promising alternative for more effective skin cancer treatment.

Low retention of NLCs on the skin presents a challenge for their topical applications. To overcome this, formulating a gel with NLCs can enhance skin retention and improve therapeutic efficacy in skin cancer treatment. One widely used gelling agent for this purpose is Carbopol-934.<sup>14</sup> Carbopol-934 serves as an effective gelling agent due to its ability to undergo cross-linking, which entraps water and forms a gel-like structure. Neutralizing a hydrated Carbopol solution allows the polymer chains to swell and create a three-dimensional network, stabilizing the gel matrix and improving NLC retention on the skin.<sup>27,28</sup> This prolonged contact time facilitates sustained drug release, optimizing delivery and therapeutic outcomes in skin cancer treatment.

The current study aims to formulate an ABZ NLC gel for transdermal application in treating skin cancer. We developed

and optimized ABZ-loaded NLCs, evaluating their ABZ content, *in vitro* release, and anti-cancer efficacy. The optimized ABZ NLCs were then incorporated into a Carbopol-934 gel and subjected to various *ex vivo* and *in vitro* analyses. This NLC-based gel formulation is expected to enhance skin permeation, enable controlled and targeted drug release at the cancer site, and reduce systemic adverse reactions associated with ABZ in patients with skin cancer.

## Materials and methods

### Materials

Albendazole was collected from Zydus, Gujarat. Compritol was obtained as a gift sample from Gattefosse India Pvt Ltd. Polysorbate 80 (Tween-80), olive oil, and polyethylene glycol (PEG)-400 were purchased from Molychem, Mumbai. All remaining chemicals utilized were of analytical quality.

### Cell culture

The skin cancer (B16F10) cell line and human epidermal cells (HaCaT) were procured from ATCC, USA. Stock cells were cultured in DMEM supplemented with 10% inactivated fetal bovine serum (FBS), penicillin ( $100 \text{ IU mL}^{-1}$ ) and streptomycin ( $100 \mu\text{g mL}^{-1}$ ) under a humidified atmosphere of 5%  $\text{CO}_2$  at  $37^\circ\text{C}$  until confluent.

### Methods

**Screening study.** The composition of NLCs encompasses co-surfactants, surfactants, and solid and liquid lipids. The solubility of ABZ in various formulation components was considered while choosing those components. The visual assessment of ABZ solubility within solid lipids involved placing a consistent quantity of 1 mg of ABZ into a test tube containing melted solid lipids in 50 mg increments. Following ABZ addition, the test tube was visually checked to confirm complete ABZ dissolution.<sup>12</sup> By mixing an excess of ABZ (2 mg) with a predetermined weight of liquid lipids (600.0 mg) in a glass test tube, the solubility of ABZ in various liquid lipids was investigated. The glass test tubes were kept at  $37 \pm 0.5^\circ\text{C}$  in a shaker for 72 h. After the tubes were centrifuged, the quantity of ABZ in the supernatant was measured by a spectrophotometric technique at 305 nm. The solubility of ABZ in surfactants and co-surfactants (1% w/v aqueous solution) was measured in a similar manner to that mentioned above.<sup>12</sup>

**Fabrication and optimization of ABZ-loaded NLCs.** ABZ-loaded NLCs were developed employing the hot melt-emulsification ultrasonication approach.<sup>23,24</sup> The measured quantity of solid lipid (glyceryl monostearate; GMS) and liquid lipid (oleic acid) in a 1 : 1 ratio were added to a co-surfactant (polyethylene glycol; PEG-200) and heated at  $5^\circ\text{C}$  above the melting point of GMS. In the oil phase prepared above, the required quantity of ABZ was dissolved. In the interim, the aqueous phase comprised of Tween-80 was subjected to a temperature equal to that of the lipid phase. The ratio of Tween-80 and PEG-200 employed in NLC fabrication was 2 : 1. Using a magnetic



**Table 1** Experimental runs developed using BBD

Formulation code	Factor 1 $X_1$ : $O_{\text{mix}}$ conc. (%)	Factor 2 $X_2$ : $S_{\text{mix}}$ conc. (%)	Factor 3 $X_3$ : probe cycle number	Response 1 $Y_1$ : EE (%)	Response 2 $Y_2$ : particle size (nm)
A1	2.5	27.5	30	69.55	187.3
A2	2.5	28.5	20	75.5	338.4
A3	1.5	26.5	30	52.6	159.8
A4	3.5	28.5	30	85.6	391.4
A5	2.5	26.5	40	55.8	182.2
A6	3.5	26.5	30	68.85	340.1
A7	2.5	27.5	30	70.25	196.9
A8	2.5	26.5	20	79.65	280.4
A9	1.5	27.5	40	44.72	146.5
A10	2.5	27.5	30	72.4	187.3
A11	1.5	27.5	20	44.72	167.3
A12	3.5	27.5	20	81.35	469.5
A13	3.5	27.5	40	65.35	209.7
A14	2.5	27.5	30	73.75	186
A15	2.5	27.5	30	74.15	183.5
A16	2.5	28.5	40	89.85	176.5
A17	1.5	28.5	30	51.45	147.7

stirrer, the aqueous phase was dropwise added to the lipid phase while being stirred at 1000–1200 rpm. Later, the formulation was homogenized using a probe sonicator (Dakshin Pvt Ltd, Mumbai) for 30 min at a 75% amplitude frequency and chilled to achieve ABZ NLCs.<sup>25</sup>

**Formulation optimization.** Utilizing Box-Behnken Design (BBD) through Design Expert Software Version 13.0 (Stat-Ease Inc., Minneapolis, USA), the ABZ NLCs were optimized. The software created a total of 17 experimental runs (Table 1), focusing on exploring the impacts of independent factors, namely  $O_{\text{mix}}$  concentration ( $X_1$ : 1.5–3.5%),  $S_{\text{mix}}$  concentration ( $X_2$ : 26.5–28.5%), and probe cycle number ( $X_3$ : 20–40 cycles), on the entrapment efficiency (%EE;  $Y_1$ ) and particle size ( $Y_2$ ). The data collected were evaluated using analysis of variance (ANOVA). Ultimately, the formulation was optimized by utilizing the desirability function.<sup>19</sup>

### Characterization of NLCs

**% Entrapment efficiency (%EE) and % drug loading capacity (%DLC).** To estimate the quantity of untrapped ABZ from NLCs ( $E_2$ ), an Eppendorf tube (2.0 mL) was filled with 0.5 mL of ABZ NLCs and centrifuged at 10 000 rpm for 90 min in a cooling centrifuge machine. Afterward, 0.1 mL of the supernatant was diluted with 5.0 mL of methanolic hydrochloride and analyzed using a UV spectrophotometer at 308 nm. Similarly, the total quantity of ABZ present in NLCs was estimated by diluting ABZ NLCs (0.5 mL) with methanolic hydrochloride (4.5 mL). This solution was subjected to sonication for around 10 min and analyzed using a UV spectrophotometer at the same wavelength. Finally, the %EE was calculated using the below formula:

$$\%EE = \frac{(E_1 - E_2)}{E_1} \times 100$$

$$\%DLC = \frac{\text{ABZ entrapped}}{\text{Total lipid}} \times 100$$

**Mean particle size and zeta potential.** The particle size of NLCs indicates their skin permeability upon topical application, whereas the zeta potential is related to the stability of the formulation. By employing a Horiba Zetasizer (HORIBA SZ-100, Japan), the mean particle size and zeta potential of the ABZ NLC formulation were measured in triplicate. Mean  $\pm$  SD was used to express the outcomes.<sup>12</sup>

**Scanning electron microscopy (SEM).** This study was conducted to determine the surface morphology of ABZ NLCs using SEM (JSM6100, JEOL, New Delhi, India) comprised of an image analyzing system (AnalySIS, SIS Software GmbH, Muenster, Germany). The sufficiently diluted suspension of ABZ NLCs was placed on the grid and dried, and images were captured.

**Fourier-transform infrared (FTIR) spectroscopy.** An FTIR study was conducted with the aim of assessing the compatibility between the ABZ and NLC components. Using an FTIR spectrophotometer (Bruker, Alpha II ATR Technique, Japan), the FTIR spectra of pure ABZ, GMS, oleic acid, PEG-200, and a physical mixture of ABZ with GMS, oleic acid, and PEG-200 were recorded.

**Differential scanning calorimetry (DSC).** A DSC investigation was carried out to evaluate the behavior of the samples under thermal events. DSC analysis was performed on several sample types, including pure ABZ, pure GMS, and a physical mixture of ABZ and GMS in a ratio of 1 : 1, using a PerkinElmer DSC 6000 instrument. The sample (5 mg) was hermetically sealed and then heated at a rate of 10 °C per minute under a nitrogen atmosphere.<sup>12</sup>

**Preparation of the ABZ NLC-based gel.** The ABZ NLC-based gel formulation was prepared using an optimized concentration (1.0%) of Carbopol-934. The optimized ABZ-loaded NLCs were mixed with 1.0% Carbopol-934 *via* constant agitation at 1200 rpm using a magnetic stirrer (Remi Motors Ltd, India) for 60 min. The final ABZ NLC-based gel formulation was left to swell overnight. Lastly, triethanolamine was introduced at a 0.05% w/w proportion to adjust the pH. A conven-



tional gel of ABZ was manufactured utilizing the same concentration of Carbopol-934.<sup>12,26,27</sup>

### Characterization of the ABZ NLC-based gel

**Physical properties and pH.** The ABZ-laden NLC-based gel and the conventional gel were investigated for color, homogeneity, phase separation, and pH. 1 g of each gel was added into 100 mL of distilled water separately and the pH was measured using a digital pH meter in triplicate.<sup>12</sup>

**Particle size and zeta potential.** A Horiba Zetasizer was utilized to assess the particle size and zeta potential of the conventional and ABZ NLC-based gels. Briefly, 10 mg of gel was diluted with 100 mL of distilled water and analyzed *via* the Horiba Zetasizer.<sup>12</sup>

**Rheological study.** A Brookfield rheometer equipped with a cone and plate was used to determine the viscosity of the ABZ NLC gel and the ABZ conventional gel. The measurements were performed at a rotation speed of 5 rpm and a temperature of 25 °C ± 2 °C using spindle number 7.<sup>26</sup>

**Swelling index.** The swelling index is indicative of the swelling potential of the gel. The swelling capacity of the ABZ NLC-loaded gel and the ABZ conventional gel was evaluated. A Petri dish containing 1 g of each gel formulation in porous aluminium foil was submerged in 10.00 mL of distilled water. The NLC-loaded and conventional gel samples were withdrawn at different intervals, carefully patted dry to remove excess water, and weighed. The swelling index was determined using the following formula:<sup>12</sup>

$$\text{Swelling index (\%)} = [(W_t - W_0)/W_0] \times 100$$

$W_t$ : swollen gel weight at time  $t$  and  $W_0$ : initial gel weight (at zero time).

**Spreadability study.** Spreadability is a crucial factor for topical formulations, which indicates the ease of spreadability of formulations. NLC gels should possess adequate spreading ability upon topical application. The “slip” and “drag” attributes of the gel were employed to determine its spreadability. 1.0 g of the ABZ NLC-loaded gel and the ABZ regular gel was placed on the bottom glass slide within the designated circle and then a second glass slide was laid on top of it. The upper slide was loaded with 500 g of weight, and the time that it took for the gels to spread over the designated distance was noted and spreadability was calculated.<sup>26,27</sup>

$$\text{Spreadability (S)} = \frac{\text{Weight placed on the top slide (M)} \times \text{length of the glass slide (L)}}{\text{spreading time (T)}}$$

**Texture analysis.** The texture of a topical formulation plays a crucial role in patient acceptance and compliance. The texture parameters, including adhesiveness, cohesiveness, hardness, and springiness, provide valuable insights into how a gel will feel when applied to the skin. To evaluate the texture profiles of the NLC-based gels, a TA.XT Plus Texture Analyzer (Stable Micro Systems, London, UK) was employed. Briefly, an analytical probe measuring 1.2 cm in diameter was squeezed twice at a rate of 30 mm min<sup>-1</sup>, with a recovery period of 15 s between

the completion of the first compression and the start of the second, into the ABZ NLC-based gel that had been fixed to a depth of 15 mm. The gel was analyzed at a trigger force of 4 g and a temperature of 37 °C three times.<sup>28</sup>

***In vitro* drug release.** The release behaviour of the formulations at tumor and skin pH was examined using an *in vitro* release study. The release profiles of ABZ *in vitro* from the ABZ NLCs, ABZ NLC gel, and pure ABZ dispersion were determined at pH 6.8 (tumor pH). Additionally, as NLC-based gels are intended for topical application, the release profile of ABZ from the NLC-based gel and the ABZ conventional gel was also evaluated at pH 5.5 (skin pH) using a dialysis bag method. Briefly, the pure dispersion of ABZ (3 mg), ABZ NLCs, the ABZ NLC gel, and the conventional ABZ gel (equivalent to pure ABZ of 3 mg) were separately introduced in a dialysis bag (MWCO: 12 000 Da; Sigma, Mumbai). The end sealed dialysis bags were placed in phosphate buffered saline (PBS; pH 6.8, and 5.5) kept at 37 ± 2 °C and maintained at 100 rpm. At time intervals of 0.5, 1, 2, 4, 6, 8, 18, 36, and 48 h, 1 mL of PBS was withdrawn and the same volume of fresh PBS was reintroduced to maintain the sink condition. The ABZ released at specific time intervals was estimated through an analytical method ( $n = 3$ ).<sup>12,29,30</sup>

***Ex vivo* skin permeation.** An *ex vivo* permeation study was conducted to understand the performance of the formulations after topical application. Goat ear skin was prepared for the experiment by cleaning it with cold water and removing the hair using depilatory cream.<sup>12,31</sup> The skin was then placed between the donor and acceptor compartments of a Franz diffusion cell apparatus, exposing an area of 0.785 cm<sup>2</sup>. 1 g of ABZ NLCs, ABZ NLC gel, and conventional ABZ gel was placed on the skin region separately. 1.0 mL of aliquot was taken at particular time points for 8 h and analyzed using a UV-visible spectrophotometer.

***In vitro* cytotoxicity.** The anti-cancer potential of pure ABZ, ABZ NLCs, and ABZ NLC gel was assessed against the B16F10 skin cancer cell line and HaCaT cells (human epidermal cells) using the MTT assay, as described in a previous study.<sup>12,32</sup> The cytotoxic effects of the aforesaid formulations on B16F10 cells were evaluated following overnight incubation at varying concentrations. The B16F10 cells were then brought in contact with a solution of MTT for 4.0 h and subsequently with DMSO. The liquid present at the top layer was then eliminated, and the formazan crystals generated in viable B16F10 cells were dissolved in DMSO (100 μL). The absorbance of the resulting solution was noted at 570 nm using a microplate reader, and the IC<sub>50</sub> values were calculated.<sup>12</sup>

**Stability study.** To evaluate the long-term stability of the optimized ABZ NLCs and ABZ NLC gel, a stability study was conducted following the ICH stability study guidelines Q1A (R2). The formulations were placed into plastic bottles and transparent glass vials, firmly sealed, and kept for three months at 4 °C ± 2 °C.<sup>12</sup> The %EE, particle size, and PDI were considered in evaluating ABZ NLC stability, while the appearance, pH, and viscosity of the ABZ NLC gel were determined at 1, 2, and 3 months to check its stability.





## Results and discussion

### Screening study

The solubility of ABZ in different NLC components is shown in ESI Fig. S1.† ABZ exhibited the highest solubility in GMS and oleic acid. Consequently, GMS and oleic acid were selected as the solid and liquid lipids, respectively. The highest solubility of ABZ in the above-mentioned lipids is capable of augmenting loading and guaranteeing that ABZ stays encased in the system for an extended period without prematurely leaking out.<sup>12</sup> Lipophilic ABZ is more soluble in Tween-80 owing to its lengthier aliphatic tail, which endows it with higher lipophilic properties.<sup>33</sup> Conversely, the shorter aliphatic tails of Tween-20 contribute to its more hydrophilic nature, resulting in the lowest solubility of lipophilic ABZ. Among the co-surfactants, PEG-200 demonstrated higher ABZ solubility than PEG-400 and PEG-600 due to their lower hydrophilic nature in comparison with PEG-400 and PEG-600.<sup>12</sup> In this study, the surfactant and co-surfactant with the highest ABZ solubility were chosen. Tween-80 and PEG-200 exhibited the highest ABZ solubility and were therefore selected as the surfactant and co-surfactant, respectively.

### Development, optimization, and characterization of ABZ-loaded NLCs

The melt-emulsification ultrasonication method was employed for developing ABZ NLCs while BBD was used for their optimization.

### Fitting of data to the model

Utilizing multiple linear regression analysis (MLRA) within Design Expert Software Version 13.0 (Stat-Ease Inc., Minneapolis, USA), the experimental data were fitted to estimate both main and interaction effects. The polynomial equation was generated, considering model coefficients with  $p < 0.05$ . The reliability of the model was validated by assessing various metrics, including the coefficient of correlation ( $R^2$ ) and predicted error sum of squares (PRESS), and conducting a lack of fit analysis.

Surface response analysis was conducted through 3D surface response plots to elucidate the relationship between factors, responses, and potential interaction effects. Employing numerical optimization techniques alongside the desirability function, efforts were made to achieve the optimal %EE and particle size, adhering to predetermined acceptance criteria of minimizing the particle size while maximizing the %EE. Additionally, graphic optimization was carried out to delineate the analytical design space and determine the position of the optimized solution. A total of 17 runs were produced and examined (Table 1). The quadratic models emerged as the best fits for responses  $Y_1$  ( $R^2$ : 0.9817) and  $Y_2$  ( $R^2$ : 0.9960), respectively. Further evaluation of the significance and effectiveness of the model was conducted using ANOVA, with specific outcomes presented in ESI Table S1.†

The significance of model terms was confirmed by observing probability ( $p$ ) values  $< 0.05$ . The  $F$ -values, indicating the

overall significance of the models, were determined to be 41.61 and 191.41 for response variables  $Y_1$  and  $Y_2$ , respectively. Regarding the goodness of fit, the adjusted  $R^2$  values were found to be 0.9581 and 0.9908 for responses  $Y_1$  and  $Y_2$ , respectively, while the predicted coefficient of correlation ( $R^2$ ) values were 0.7870 and 0.9458. It is worth noting that the predicted coefficient of correlation ( $R^2$ ) showed reasonable agreement with the adjusted coefficient of correlation ( $R^2$ ) for both responses  $Y_1$  and  $Y_2$  with a difference of less than 0.2. Adequate precision values of 20.28 ( $Y_1$ ) and 47.22 ( $Y_2$ ) were obtained, with values larger than 4 generally preferred.

The polynomial equations presented below elucidate the relationships of dependent and independent variables:

$$Y_1 = +72.02 + 13.08X_1 + 5.69X_2 - 3.56X_3 + 4.47X_1X_2 - 4.75X_1X_3 + 9.55X_2X_3 - 12.16X_1^2 + 4.76X_2^2 - 1.58X_3^2 \quad (1)$$

$$Y_2 = +188.20 + 98.68X_1 + 11.19X_2 - 67.84X_3 + 15.85X_1X_2 - 59.75X_1X_3 - 16.43X_2X_3 + 37.96X_1^2 + 33.59X_2^2 + 22.09X_3^2 \quad (2)$$

The increase in %EE with higher concentrations  $O_{\text{mix}}$  and  $S_{\text{mix}}$  could be attributed to enhanced solubilization and stabilization of the drug within the formulation. It is possible that a higher  $O_{\text{mix}}$  concentration provides a more extensive oil phase, allowing greater drug partitioning, thereby increasing %EE. Similarly, elevated  $S_{\text{mix}}$  concentrations might reduce interfacial tension and contribute to the formation of a more stable emulsion, which could minimize drug leakage into the aqueous phase. This combination may result in a potential improvement in the overall %EE. The effects of these variables on responses were further elucidated through 3D-response surface plots (Fig. 1).

The significance of the planned models was aptly illustrated by plotting predicted values against actual values (Fig. S2†). Additionally, model diagnosis plots (Fig. S3A, S3B† for response  $Y_1$ ; Fig. S3C, S3D† for response  $Y_2$ ) were constructed, incorporating normal and residual *versus* run plots. Upon closer inspection, it became evident that the residuals generally adhere to a straight line, indicating an even distribution of errors. This reaffirms the adequacy of the model fit, which is crucial for validating the normality assumption and ensuring the suitability of the model for process optimization. The almost equal scatter on each side of the X-axis further validates the appropriateness of the recommended models. Perturbation plots were employed to confirm the quadratic effects of variables on both the responses  $Y_1$  (Fig. S3A†) and  $Y_2$  (Fig. S3B†). These plots provide additional insight into the influence of variables on the response variables, further supporting the efficacy of the established models.

### Optimization of the formulation

The formulation optimization process employed the desirability function approach, aiming to optimize the %EE at the highest constraint and the particle size at the lowest con-





Fig. 1 3D response surface plots explaining the effects of independent variables on the %EE and particle size.

straint. A batch, formulated with 2.62%  $O_{mix}$ , 28.5%  $S_{mix}$ , and 40 probe cycles, was projected to yield a %EE of 88.31% and a mean particle size of 178.47 nm.

Subsequently, the optimized batch demonstrated a %EE and a particle size of  $89.85 \pm 5.6\%$  and  $176.5 \pm 7.3$  nm, respectively, with a polydispersity index (PDI) of  $0.41 \pm 0.06$  (Fig. 2). The plots of numerical optimization and graphical optimization are depicted in Fig. S4A and S4B,<sup>†</sup> respectively. These visual representations provide insights into the optimization process and validate the effectiveness of the chosen approach in achieving the desired formulation goals. The predicted and actual values for an individual response of the optimized ABZ NLC formulation were in close understanding with minimal bias ( $<1$ ), implying the validity and accuracy of the fabricated model as well as the powerful correlation between the variables.

### Entrapment efficiency, drug loading capacity, particle size, and zeta potential

The optimized ABZ NLCs displayed a %EE of  $89.85 \pm 5.6\%$  and a % drug loading capacity of  $3.19 \pm 0.10\%$ . These NLCs exhibited a mean particle size of  $176.5 \pm 7.3$  nm (Fig. 2a), a PDI of  $0.41 \pm 0.06$ , and a zeta potential of  $-22.7 \pm 2.3$  mV (Fig. 2b). The PDI was determined to be  $<0.5$ , indicating a high level of consistency in particle size distribution.<sup>12</sup>

### SEM

The SEM image of the ABZ NLCs (Fig. 2c) displayed spherical particles. The particle size of NLCs obtained in the SEM analysis was higher than those achieved with the Horiba particle size analyzer. The aggregate formation during the processing or storage of the freeze-dried NLC formulation could be a reason behind the increased particle size. The aggregates within the NLCs might consist of solid lipid NPs and liquid lipid domains, potentially creating spherical structures. The spherical nature of the aggregates, combined with the presence of amorphous regions from liquid lipids, increases the available surface area for drug interaction. The irregularities within the solid lipid matrices provide additional space for drug molecules, enhancing their solubility. These characteristics might provide additional binding sites for ABZ, enhancing its solubility. Furthermore, the mixed lipid matrix could prevent drug expulsion during crystallization, allowing for better retention and bioavailability. Overall, the unique types and shapes of aggregates within the NLC system may significantly contribute to improved drug solubility, highlighting the effectiveness of NLCs for drug delivery.

### FTIR analysis

The FTIR spectra of pure ABZ, GMS, oleic acid, PEG-200, and their physical mixture are depicted in Fig. 3. In the FTIR



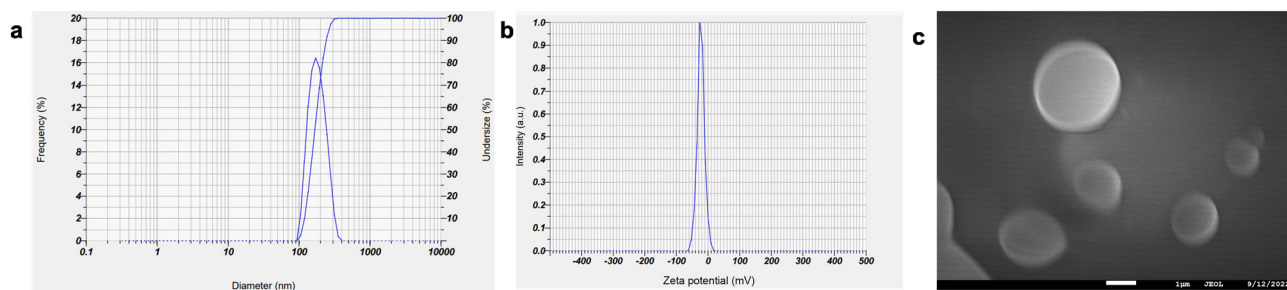


Fig. 2 Optimized ABZ NLCs: (a) mean particle size, (b) zeta potential, and (c) SEM micrograph.



Fig. 3 FTIR spectra of (a) ABZ, (b) GMS, (c) oleic acid, (d) PEG-200, and (e) the physical mixture of the ABZ and NLC components.

spectra of pure ABZ (Fig. 3a), the peaks observed at 3326, 2931, 2860 and 2663  $\text{cm}^{-1}$  are attributed to the characteristic peaks of N-H stretching, C-H aliphatic stretching, and N-H stretching in imidazole, respectively. Moreover, the peaks at 1712  $\text{cm}^{-1}$  and 1525  $\text{cm}^{-1}$  are the peaks corresponding to the bending vibration of the O=C bond in carbamate and the stretching vibration of the C=N group in ABZ.<sup>34</sup> All the dis-

tinctive peaks of pure ABZ were noticed in the FTIR spectra of the physical combination of the ABZ and NLC components (Fig. 3e), suggesting compatibility between them.

#### DSC

A DSC thermogram of pure ABZ and GMS (Fig. 4a and b) demonstrated prominent endothermic peaks at 219.08 °C and





Fig. 4 DSC thermogram of (a) ABZ, (b) GMS, and (c) the physical mixture of ABZ and GMS.

59.23 °C which correspond to the melting point of ABZ and GMS, respectively. In the DSC thermogram of the physical combination of ABZ and GMS (Fig. 4c), melting endothermic peaks were noticed at 59.01 °C and 201.19 °C. Thus, no endothermic peak corresponding to ABZ was observed, indicating the existence of ABZ under the conditions of the molecules in lipids.<sup>35</sup>

### Preparation of the ABZ NLC gel

The ABZ NLC gel was fabricated by incorporating Carbopol-934 at several concentrations (0.5, 1.0, 1.5, and 2.0% w/v). Interestingly, the gel prepared with 1.0% w/v Carbopol 934 exhibited greater consistency (viscosity:  $6.64 \pm 0.67$  Pa s) compared to the gel prepared with other concentrations of Carbopol-934. Based on the observed consistency and viscosity, Carbopol-934 at 1.0% w/v emerged as the optimal concentration for the ABZ NLC gel formulation. Therefore, this concentration was chosen for further studies.<sup>12,36</sup>

### Characterization of the optimized ABZ NLC gel

**Physical properties and pH.** The optimized gel formulation was found to be white in color with a clear or elegant appearance, along with a uniform texture. Furthermore, the pH of the gel was observed within the range of 5.1–6.0, which aligns with the natural pH of the skin. This similarity in pH suggests that the gel could potentially promote smooth ABZ penetration into the skin without triggering any irritation.<sup>37</sup>

**Mean particle size and zeta potential.** The ABZ-NLC gel showed particles with a size of  $220.2 \pm 7.4$  nm and a PDI of  $0.37 \pm 0.04$  (Fig. 5a), while the conventional ABZ gel had the largest particle size at  $311.6 \pm 9.4$  nm with a PDI of  $0.47 \pm 0.19$  (Fig. 5b). This increase in the particle size of ABZ NLCs following incorporation into the gel could be attributed to the adsorption of a gelling agent on the surface of NLCs, leading to a three-dimensional polymeric structure surrounding the NLC surface.<sup>38</sup> The zeta potentials of the ABZ-NLC gel and the regular ABZ gel were observed to be  $-32.5 \pm 4.2$  mV and  $-23.4 \pm 3.2$  mV, respectively (Fig. 5c and d). The particle size of the ABZ-NLC gel was significantly smaller than that of the regular gel, reflecting the inherent size advantage of NLCs. Regardless, the overall smaller size of the NLC-based gel compared to the conventional gel suggests improved skin permeation of ABZ. Moreover, the lower PDI values of both gels ( $<0.5$ ) indicate greater uniformity in size distribution, potentially contributing to better stability and reproducibility.<sup>39</sup> Finally, the high zeta potential values (close to  $\pm 30$  mV) observed for the gels are indicative of enhanced colloidal stability, minimizing aggregation and ensuring long-term shelf life.<sup>40</sup>

**Rheological study.** Viscosity plays a pivotal role in transdermal applications, impacting aspects like simplicity of application, spreadability, payload release, and gel stability. The measured viscosity values of the ABZ NLC-loaded gel and the ABZ conventional gel were  $6.64 \pm 0.67$  Pa s and  $14.75 \pm 2.4$  Pa s, respectively. Our findings align with reported viscosity values for topical liposomal gels developed for cancer treatment.<sup>41</sup>

**Swelling index.** The ABZ NLC gel and the ABZ regular gel exhibited swelling capacities of  $26.22 \pm 1.5\%$  and  $21.32 \pm 1.1\%$ , respectively. Carbopol is a swellable gelling agent that forms a hydrogen bond with water by changing the carboxylic acid group ( $-\text{COOH}$ ) into the carboxylate group ( $\text{COO}^-$ ). The hydrophilic polymer matrix in both gels, which controls water intake and expansion, ultimately causes swelling. There is a direct correlation between the concentration of Carbopol and the swelling index. The NLCs introduce slight physical hindrances due to the change in lipophilicity of lipidic components but does not significantly alter the swelling behavior, which may be caused by the same pH and Carbopol concentration of the formulation.<sup>42</sup> These values fall within the acceptable range documented in prior research, suggesting adequate water uptake potential for sustained drug release.<sup>26,27</sup>

**Spreadability.** The spreadability of the NLC-based gel significantly impacts its performance, influencing how it interacts with the skin and delivers the incorporated cargo. The spreadability of the ABZ NLC gel was found to be  $14.2 \pm 0.8$  g  $\text{cm s}^{-1}$ . Conversely, the conventional ABZ gel displayed a noticeably lower spreadability of  $4.6 \pm 0.3$  g  $\text{cm s}^{-1}$ . This lower spreadability of the conventional gel stems from its higher viscosity, which makes it less easy to glide over the skin. The observed spreadability of NLC-based gels falls within the favorable range reported in a previous study,<sup>26,27</sup> indicating their potential for smooth application and optimal treatment outcomes.







Fig. 5 Mean particle size of (a) the ABZ NLC gel and (b) the ABZ conventional gel; zeta potential of (c) the ABZ NLC gel and (d) the ABZ conventional gel.

**Texture analysis.** Texture analysis was conducted on the NLC-based gel to evaluate key sensory characteristics such as adhesiveness, cohesiveness, hardness, and springiness, all of which play an important role in patient acceptance of topical formulations. The results are presented in ESI Fig. S5.† Gel hardness reflects ease of application, while adhesiveness measures how well the gel sticks to the skin. The hardness values of the ABZ NLC gel and the ABZ conventional gel were  $23.90 \pm 3.9$  and  $35.40 \pm 4.8$  mJ. The hardness of the ABZ NLC gel was less than that of the conventional gel, suggesting excellent spreadability and convenience of withdrawal from the container. Moreover, the adhesiveness, hardness and cohesiveness values of the ABZ NLC gel were  $3.72 \pm 0.8$  mm,  $1.40 \pm 0.06$  mJ, and  $0.96 \pm 0.05$ , respectively. The conventional ABZ gel displayed springiness, adhesiveness, and cohesiveness values of  $3.0 \pm 0.6$  mm,  $3.10 \pm 0.7$  mJ, and  $0.45 \pm 0.02$ , respectively. These findings indicate that the NLC-based gel offers enhanced adhesion and prolonged skin contact compared to conventional formulations, as supported by previous reports.<sup>12,43</sup> This improved sensory profile can significantly contribute to patient satisfaction and adherence to the treatment regimen.

**In vitro ABZ release.** ABZ release from the plain ABZ dispersion, ABZ NLCs, and the ABZ NLC-based gel in PBS pH 6.8

was conducted to investigate tumor targeting behaviour (Fig. 6a). The pure ABZ dispersion demonstrated a release rate of  $20.4 \pm 1.7\%$  in 48 h. The release rates of ABZ from NLCs and the NLC gel were found to be  $93.1 \pm 7.6\%$  and  $80.8 \pm 6.5\%$ , respectively, in 48 h. Interestingly, at acidic pH 6.8, the release profile of ABZ was significantly higher ( $p < 0.05$ ) and sustained compared to both NLCs and the NLC-based gel. This higher release at acidic pH could be attributed to the weakening of the structural integrity of NLCs due to altered lipid conformation, leading to increased diffusion and release of encapsulated ABZ.<sup>12</sup> This pH-sensitive release pattern highlights the potential of these NLCs and the NLCs-based gel to deliver ABZ specifically to tumors, which often exhibit acidic microenvironments. Overall, the controlled release from these systems offers a promising approach for tumor targeting.<sup>12</sup>

Furthermore, in PBS pH 5.5, the ABZ release was  $84.6 \pm 6.6\%$  from the NLC-based gel and  $33.7 \pm 3.6\%$  from the conventional gel, respectively, after 48 h (Fig. 6b). Thus, the ABZ release from the NLC gel was remarkably greater than that from the ABZ conventional gel. This increased ABZ release at acidic pH could be attributed to the weakening of the NLC-based gel structural integrity.<sup>12</sup> Moreover, the regulated release





Fig. 6 *In vitro* release profile of formulations (a) in PBS pH 6.8 and (b) in PBS pH 5.5.

of ABZ from the NLC-based gel may be attributed to the gradual diffusion of ABZ from the matrix comprised of lipids and gel.<sup>44</sup>

**Ex vivo skin permeation.** A study of *ex vivo* skin permeation of ABZ was conducted using goat ear skin, comparing the efficacy of NLCs, the NLC-based gel, and the conventional gel formulation. The permeability of ABZ through goat ear skin from ABZ NLCs was found to be  $205 \pm 2.7 \mu\text{g cm}^{-2}$ , with a flux of  $6.2 \mu\text{g cm}^{-2} \text{ h}^{-1}$ . In contrast, the ABZ NLC gel exhibited a permeability of  $180 \pm 2.2 \mu\text{g cm}^{-2}$  and a flux of  $5.5 \mu\text{g cm}^{-2} \text{ h}^{-1}$ . In comparison, the permeability of ABZ from the conventional gel was significantly lower, recorded at  $40 \pm 1.7 \mu\text{g cm}^{-2}$  with a flux of  $1.27 \mu\text{g cm}^{-2} \text{ h}^{-1}$  (Fig. 7). Notably, the permeation of ABZ from ABZ NLCs and the ABZ NLC gel was found to be 5.1 and 4.5 times greater, respectively, than that observed with the conventional gel. This marked enhancement in ABZ permeation from the NLC-based formulations can be attributed to several factors. The nanoscale dimensions of the NLCs increase the solubility and dissolution rate of ABZ, allowing for more effective drug absorption through the skin barrier. Smaller particle size enhances the surface area for drug release and interaction with the skin. Additionally, the smaller particle size of the NLC-based gel facilitates greater contact with the skin surface, which enhances drug delivery by

maximizing the interaction between the formulation and the *stratum corneum*. Furthermore, the disruption of the *stratum corneum* lipid structure by the NLCs may promote enhanced permeability, as the lipid nanoparticles can fluidize the skin lipids, further aiding in drug diffusion. Overall, these findings highlight the significant potential of NLCs and NLC-based gels as effective delivery systems for enhancing the transdermal permeation of ABZ, surpassing conventional gel formulations.<sup>12</sup>

**In vitro cytotoxicity.** Each formulation, when confronted with the B16F10 melanoma cell line, exhibited cytotoxic effects that scaled with the ABZ concentration. The  $\text{IC}_{50}$  values of pure ABZ, ABZ NLCs, and the ABZ NLC gel were determined to be  $3.18 \pm 0.34 \mu\text{M}$ ,  $1.87 \pm 0.10 \mu\text{M}$ , and  $4.13 \pm 0.75 \mu\text{M}$ , respectively, against B16F10 cells following 48 h of incubation. The cytotoxicity of ABZ NLCs was noticeably greater (1.7-fold higher than that of pure ABZ) and (2.2-fold higher than that of the ABZ NLC gel), respectively. This significant rise in cytotoxicity of ABZ NLCs could be attributed to increased intracellular (endocytosis-mediated uptake by cells) in the cancer cell.<sup>45</sup> Furthermore, the decrease in cytotoxicity (higher  $\text{IC}_{50}$  value) of ABZ loaded into the NLC-based gel may be due to its controlled cargo release from the ABZ NLC-based gel. The presence of the polymer gel matrix likely slows down ABZ release from the NLC-based gel, delaying its encounter with cancer cells and thereby mitigating its toxic impact.<sup>12</sup> No  $\text{IC}_{50}$  values were detected in HaCaT cells treated with the above-mentioned formulations (reduction in cell viability was less than 15%).<sup>46</sup> Thus, negligible or lack of cytotoxicity against HaCaT cells indicates the biocompatibility of the developed formulations against HaCaT normal cells.

**Stability.** The ABZ within the NLCs remained especially stable, with 80–90% of EE after three months of cold storage. Minimal 1–4% deterioration was found throughout this time, demonstrating the good stability of ABZ NLCs. The particle size remained constant, falling within the constrained range of 160–200 nm, with a PDI of 0.103–0.398. Thus, no significant change in the %EE and particle size of ABZ NLCs was found following three months of storage, demonstrating the exceptional stability of NLCs in cold temperatures.



Fig. 7 *Ex vivo* permeation of formulations in PBS pH 7.4.



The ABZ NLC-based gel was observed to be white, elegant, pleasing, and homogeneous in consistency. This gel had rather constant pH levels, ranging from 5.4 to 6.0. Furthermore, the viscosity (6.32–6.64 Pa s) of the gel after three months was close to that of the fresh formulation. The NLC-based gel viscosity, pH, and physical appearance all remained essentially the same, which is evidence of its exceptional stability.

## Conclusion

This study investigated the potential of ABZ, a repurposed anti-fungal medication for the treatment of melanoma skin cancer. Our findings displayed remarkable cytotoxicity of ABZ against the B16F10 cell line, indicating its repurposing potential against skin cancer. The optimization process involved the probe cycle number,  $S_{\text{mix}}$  concentration, and  $O_{\text{mix}}$  concentration as independent attributes and the %EE and particle size as response variables. The optimization using BBD demonstrated significant effects of independent variables on the response variables. The NLC-based gel demonstrated optimistic viscosity, physical properties, and texture attributes, signifying the aptness of the developed NLC-based gel for topical use. Moreover, the nanometer size of both ABZ NLCs and the ABZ NLC gel is indicative of its permeation through the skin. The controlled release behaviour, substantial permeation, and cytotoxicity towards B16F10 cells and the lack of toxicity towards normal HaCaT cells revealed its promise and effectiveness in localized delivery against skin cancer.

In a nutshell, compared to conventional oral or injectable chemotherapies, this localized and controlled delivery of repurposed ABZ offers a glimmer of hope. Reduced dosage and dose frequency and minimized side effects, while amplifying treatment efficacy and patient adherence – those are the promise of this innovative approach. The ABZ-loaded NLCs integrated into the gel formulation stand as a potential, safe, effective, and novel way in the fight against skin cancer. However, further investigations into the animal cancer model are of vital significance.

## Author contributions

CK: investigation, data curation, methodology and resources, and writing – original draft; KK: methodology and resources, and writing – original draft; SD: methodology and resources, and writing – original draft; AM: methodology and resources, and writing – original draft; SN: methodology, software, writing – editing; PSK: conceptualization, supervision, and writing – reviewing and editing; JD: conceptualization, supervision, and writing – reviewing and editing.

## Data availability

The data that support the findings of this study are available from the corresponding author upon reasonable request.

## Conflicts of interest

The authors declare that they have no conflict of interests.

## Acknowledgements

The authors thank Gattefosse India Pvt Ltd, for providing Compritol 888 ATO as a gift sample. We also thank Tatyasaheb Kore College of Pharmacy, Warananagar for supporting this research work.

## References

- 1 P. Kumbhar, K. Kolekar, C. Khot, S. Dabhole, A. Salawi, F. Y. Sabei, *et al.*, Co-crystal nanoarchitectonics as an emerging strategy in attenuating cancer: Fundamentals and applications, *J. Controlled Release*, 2023, **353**, 1150–1170.
- 2 R. L. Siegel, K. D. Miller, H. E. Fuchs and A. Jemal, Cancer statistics, 2021, *CA Cancer J. Clin.*, 2021, **71**(1), 7–33.
- 3 P. S. Kumbhar, V. Kamble, S. Vishwas, P. Kumbhar, K. Kolekar, G. Gupta, *et al.*, Unravelling the success of transferosomes against skin cancer: Journey so far and road ahead, *Drug Delivery Transl. Res.*, 2024, **17**, 1–20.
- 4 P. Kumbhar, K. Kole, T. Yadav, A. Bhavar, P. Waghmare, R. Bhokare, *et al.*, Drug repurposing: An emerging strategy in alleviating skin cancer, *Eur. J. Pharmacol.*, 2022, **926**, 175031.
- 5 . Available online: Skin cancer statistics | World Cancer Research Fund International (wcrf.org). <https://www.wcrf.org/cancer-trends/skin-cancer-statistics/>.
- 6 M. K. Abu Mahmoud, Improving skin cancer (melanoma) detection: New method (Doctoral dissertation).
- 7 R. I. Neves, M. Brgoch and B. R. Gastman, Treatment of squamous and basal cell carcinoma of the skin, in *Cutaneous Malignancies: A Surgical Perspective*, 2018, pp. 43–85.
- 8 C. Prieto-Granada and P. Rodriguez-Waitkus, Cutaneous squamous cell carcinoma and related entities: Epidemiology, clinical and histological features, and basic science overview, *Curr. Probl. Cancer*, 2015, **39**(4), 206–215.
- 9 D. S. Cassarino, D. P. DeRienzo and R. J. Barr, Cutaneous squamous cell carcinoma: A comprehensive clinicopathologic classification: Part two, *J. Cutaneous Pathol.*, 2006, **33**(4), 261–279.
- 10 P. Kumbhar, K. Kole, A. Manjappa, N. K. Jha, J. Disouza and V. Patravale, Drug Repurposing Opportunities in Cancer, in *Drug Repurposing for Emerging Infectious Diseases and Cancer*, Springer Nature Singapore, 2023, pp. 53–87.
- 11 W. Link, *Principles of cancer treatment and anticancer drug development*, Springer International Publishing, Cham, 2019.
- 12 P. S. Kumbhar, A. S. Manjappa, R. R. Shah, S. J. Nadaf and J. I. Disouza, Nanostructured Lipid Carrier-Based Gel for Repurposing Simvastatin in Localized Treatment of Breast Cancer: Formulation Design, Development, and In Vitro



- and In Vivo Characterization, *AAPS PharmSciTech*, 2023, **24**(5), 106.
- 13 P. Nygren and R. Larsson, Drug repositioning from bench to bedside: Tumour remission by the antihelmintic drug mebendazole in refractory metastatic colon cancer, *Acta Oncol.*, 2014, **53**(3), 427–428.
  - 14 J. S. Petersen and S. K. Baird, Treatment of breast and colon cancer cell lines with anti-helminthic benzimidazoles mebendazole or albendazole results in selective apoptotic cell death, *J. Cancer Res. Clin. Oncol.*, 2021, **147**(10), 2945–2953.
  - 15 K. R. Vandana, P. R. Yalavarthi, H. C. Vadlamudi, J. K. Kalluri and A. Rasheed, Process, physicochemical characterization and *in vitro* assessment of albendazole microcrystals, *Adv. Pharm. Bull.*, 2017, **7**(3), 419.
  - 16 R. Ossio, R. Roldan-Marin, H. Martinez-Said, D. J. Adams and C. D. Robles-Espinoza, Melanoma: A global perspective, *Nat. Rev. Cancer*, 2017, **17**(7), 393–394.
  - 17 D. Van Staden, Development of a topical self-emulsifying drug delivery system for optimised delivery (Doctoral dissertation, North-West University (South-Africa)).
  - 18 P. Kumbhar, K. Kolekar, S. Vishwas, P. Shetti, V. Kumbhar, T. D. Pinto, *et al.*, Treatment Avenues for Age-Related Macular Degeneration: Breakthroughs and Bottlenecks, *Ageing Res. Rev.*, 2024, **98**(102322), 102322.
  - 19 S. R. Parveen, S. Wadhwa, M. R. Babu, S. Vishwas, L. Corrie, A. Awasthi, *et al.*, Formulation of chrysin loaded nanostructured lipid carriers using Box Behnken design, its characterization and antibacterial evaluation alone and in presence of probiotics co-loaded in gel, *J. Drug Delivery Sci. Technol.*, 2023, **84**(104411), 104411.
  - 20 P. Kumbhar, P. Waghmare, S. Nadaf, A. Manjappa, R. Shah and J. Disouza, QbD and Six Sigma quality approach for chromatographic estimation of repurposed simvastatin from nanostructured lipid carriers, *Microchem. J.*, 2023, **185**(108310), 108310.
  - 21 V. Phatale, K. K. Vaiphei, S. Jha, D. Patil, M. Agrawal and A. Alexander, Overcoming skin barriers through advanced transdermal drug delivery approaches, *J. Controlled Release*, 2022, **351**, 361–380.
  - 22 E. B. Souto, I. Baldim, W. P. Oliveira, R. Rao, N. Yadav, F. M. Gama, *et al.*, SLN and NLC for topical, dermal, and transdermal drug delivery, *Expert Opin. Drug Delivery*, 2020, **17**(3), 357–377.
  - 23 T. A. Ismail, T. M. Shehata, D. I. Mohamed, H. S. Elsewedy and W. E. Soliman, Quality by design for development, optimization and characterization of brucine ethosomal gel for skin cancer delivery, *Molecules*, 2021, **26**(11), 3454.
  - 24 R. K. Jangde, T. Khan and H. Bhardwaj, Development and characterization of nanostructured lipid carrier for topical delivery of naringenin, *Res. J. Pharm. Technol.*, 2023, **16**, 2572–2576.
  - 25 F. Shakeel, P. Alam, A. Ali, M. H. Alqarni, A. Alshetali, M. M. Ghoneim, *et al.*, Investigating antiarthritic potential of nanostructured clove oil (*Syzygium aromaticum*) in FCA-induced arthritic rats: Pharmaceutical action and delivery strategies, *Molecules*, 2021, **26**(23), 7327.
  - 26 S. Malavi, P. Kumbhar, A. Manjappa, J. Disouza and J. Dwivedi, Emulgel for improved topical delivery of Tretinoin: Formulation design and characterization, *Ann. Pharm. Fr.*, 2022, **80**(2), 157–168.
  - 27 S. Malavi, P. Kumbhar, A. Manjappa, S. Chopade, O. Patil, U. Kataria, *et al.*, Topical Emulgel: Basic Considerations in Development and Advanced Research, *Indian J. Pharm. Sci.*, 2022, **84**, 5.
  - 28 J. Hurler, A. Engesland, B. Poorahmary Kermany and N. Škalko, –Basnet, Improved texture analysis for hydrogel characterization: Gel cohesiveness, adhesiveness, and hardness, *J. Appl. Polym. Sci.*, 2012, **125**(1), 180–188.
  - 29 M. Imran, M. K. Iqbal, K. Imtiyaz, S. Saleem, S. Mittal, M. M. Rizvi, *et al.*, Topical nanostructured lipid carrier gel of quercetin and resveratrol: Formulation, optimization, *in vitro* and *ex vivo* study for the treatment of skin cancer, *Int. J. Pharm.*, 2020, **587**(119705), 119705.
  - 30 T. Vohra, I. Kaur, H. Heer and R. R. Murthy, Nanolipid carrier-based thermoreversible gel for localized delivery of docetaxel to breast cancer, *Cancer Nanotechnol.*, 2013, **4**, 1–2.
  - 31 V. K. Rapalli, V. Kaul, T. Waghule, S. Gorantla, S. Sharma, A. Roy, *et al.*, Curcumin loaded nanostructured lipid carriers for enhanced skin retained topical delivery: Optimization, scale-up, *in vitro* characterization and assessment of *ex vivo* skin deposition, *Eur. J. Pharm. Sci.*, 2020, **152**(105438), 105438.
  - 32 L. Zhu, Q. Yang, R. Hu, Y. Li, Y. Peng, H. Liu, *et al.*, Novel therapeutic strategy for melanoma based on albendazole and the CDK4/6 inhibitor palbociclib, *Sci. Rep.*, 2022, **12**(1), 5706.
  - 33 I. Ali, S. Saifullah, F. Ahmed, S. Ullah, I. Imkan, K. Hussain, *et al.*, Synthesis of long-tail nonionic surfactants and their investigation for vesicle formation, drug entrapment, and biocompatibility, *J. Liposome Res.*, 2020, **30**(3), 255–262.
  - 34 R. Racoviceanu, C. Trandafirescu, M. Voicu, R. Ghiulai, F. Borcan, C. Dehelean, *et al.*, Solid Polymeric Nanoparticles of Albendazole: Synthesis, Physico-Chemical Characterization and Biological Activity, *Molecules*, 2020, **25**(21), 5130.
  - 35 K. D. Koradia, R. H. Parikh and H. D. Koradia, Albendazole nanocrystals: Optimization, spectroscopic, thermal and anthelmintic studies, *J. Drug Delivery Sci. Technol.*, 2018, **43**, 369–378.
  - 36 M. Slavkova, B. Tzankov, T. Popova and C. Voycheva, Gel formulations for topical treatment of skin cancer: A review, *Gels*, 2023, **9**(5), 352.
  - 37 F. Han, R. Yin, X. Che, J. Yuan, Y. Cui, H. Yin and S. Li, Nanostructured lipid carriers (NLC) based topical gel of flurbiprofen: Design, characterization and *in vivo* evaluation, *Int. J. Pharm.*, 2012, **439**(1), 349–357.
  - 38 Y. Zheng, W. Ouyang, Y. Wei, S. Syed, C. Hao, B. Wang, *et al.*, Effects of Carbopol® 934 proportion on nanoemulsion gel for topical and transdermal drug delivery: A skin permeation study, *Int. J. Nanomed.*, 2016, **11**, 5971–5987.





- 39 U. Nagaich and N. Gulati, Nanostructured lipid carriers (NLC) based controlled release topical gel of clobetasol propionate: Design and in vivo characterization, *Drug Delivery Transl. Res.*, 2016, **6**(3), 289–298.
- 40 A. K. Sachan, A. Gupta and M. Arora, Formulation & characterization of nanostructured lipid carrier (NLC) based gel for topical delivery of etoricoxib, *J. Drug Delivery Ther.*, 2016, **6**(2), 4–13.
- 41 A. Czajkowska-Kośnik, E. Szymańska and K. Winnicka, Nanostructured lipid carriers (NLC)-based gel formulations as Etodolac delivery: From gel preparation to permeation study, *Molecules*, 2022, **28**(1), 235.
- 42 M. Begum, A. Alqahtani, M. Ghazwani, M. Ramakrishna, U. Hani, A. Atiya, *et al.*, Preparation of carbopol 934 based ketorolac tromethamine buccal mucoadhesive film: in vitro, ex vivo, and in vivo assessments, *Int. J. Polym. Sci.*, 2021, **1**, 4786488.
- 43 D. Yilmaz Usta, Z. S. Teksin and F. Tugcu-Demiroz, Evaluation of Emulgel and Nanostructured Lipid Carrier-Based Gel Formulations for Transdermal Administration of Ibuprofen: Characterization, Mechanical Properties, and *Ex vivo* Skin Permeation, *AAPS PharmSciTech*, 2024, **25**(5), 124.
- 44 J. R. Madan, S. Khobaragade, K. Dua and R. Awasthi, Formulation, optimization, and in vitro evaluation of nanostructured lipid carriers for topical delivery of Apremilast, *Dermatol. Ther.*, 2020, **33**(3), e13370.
- 45 P. Kumbhar, V. Khade, V. Khadake, P. Marale, A. Manjappa, A. Nadaf, *et al.*, Ifosfamide-Loaded Cubosomes: An Approach to Potentiate Cytotoxicity against MDA-MB-231 Breast Cancer Cells, *FABAD J. Pharm. Sci.*, 2023, **48**, 37–52.
- 46 R. Podgórski, M. Wojasiński and T. Ciach, Nanofibrous materials affect the reaction of cytotoxicity assays, *Sci. Rep.*, 2022, **12**, 9047.

